Heliyon 10 (2024) e34664

Contents lists available at ScienceDirect

Heliyon

journal homepage: www.cell.com/heliyon

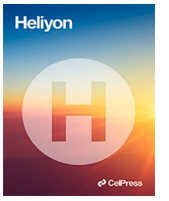

Research article

Employing dolomite as magnesium source to prepare calcined layered double hydroxides for chromium contaminated soil treatment: Exploring the influence of temperature, bioavailability, and microbial diversity

Donghua Zhang [a,*], Zhimeng Liu [b]

[a] Department of Mining Engineering, College of Mining Engineering, Taiyuan University of Technology, Taiyuan, 030024, China
[b] Shanxi Coal Institute of Planing &design (group) Co.,ltd., Taiyuan, 030024, China

ARTICLE INFO

Keywords:
Dolomite
Cr
Calcination
Immobilization
Soil
LDHs

ABSTRACT

Layered double hydroxides (LDH-D) and their calcined counterparts, using dolomite as a source of magnesium, were utilized for the immobilization of chromium (Cr(VI)) in soil. The results indicate that LDH-D, both with and without varying calcination temperatures, can effectively immobilize Cr(VI) in soil. Among the different calcination temperatures tested, LDH-D subjected to calcination at 500 °C (LDH-D-500) showed particularly high efficacy. Long-term TCLP experiments demonstrated the inhibition of soil-to-plant transmission of Cr(VI), thereby highlighting the long-lasting immobilization capacity of LDH-D and its calcined derivatives. Furthermore, the analysis of the microbial community's adaptation in post-remediation soil confirmed the durability and bioavailability of LDH-D-500 for Cr immobilization. Examination of the material's morphology and structure after immobilization shed light on the mechanism of immobilization in soil. The results revealed that interlayer anion exchange and surface adsorption were the main factors responsible for the effective immobilization of LDH-D and LDH-D-300. On the other hand, LDH-D-900, with a dominant spinel ($MgAl_2O_4$) structure, faced challenges in returning to its original layered configuration, making surface adsorption the primary mechanism for immobilization. LDH-D-500 primarily relied on the structure memory effects of LDHs to immobilize Cr(VI) through structural recovery processes, facilitated by electrostatic attraction and surface adsorption. It is also important to note that $CaCO_3$ plays an important role in adsorption. Additionally, a portion of Cr(VI) was converted to Cr(III) through phenomena such as isomer substitution and complexation adsorption. The proficiency of LDH-D-500 in immobilizing Cr, its ability for instantaneous separation, and the potential for regeneration make it a promising material for remediation of heavy metal-contaminated soil. The investigations suggest that the use of dolomite to create hydrotalcite and calcining it at 500 °C could effectively render environmental Cr inactive, thereby optimizing resource utilization.

* Corresponding author.
E-mail address: zhangdonghua@tyut.edu.cn (D. Zhang).

https://doi.org/10.1016/j.heliyon.2024.e34664
Received 15 February 2024; Received in revised form 24 June 2024; Accepted 15 July 2024
Available online 17 July 2024

1. Introduction

Modern industries such as those related to chemicals, steel, and leather often utilize chromium and its derivatives extensively. The presence of this element in groundwater, surface water, and soil has surfaced as a major environmental concern [1], marked by the United States Environmental Protection Agency (USEPA) as one of the most detrimental pollutants. Chromium is primarily found as Cr (VI) and Cr(III) in nature, with Cr(VI) noted to be compatively more mobile and considerably a hundred times more toxic than Cr(III) [2]. The swift growth experienced in the chemical industry in recent years has led to a significant discharge of chromium-infused wastewater and waste residues into the environment, and this has consequently initiated severe chromium pollution in certain water bodies and regions of soil [3]. Cr(VI), attributed with high water solubility, potent oxidizing characteristics, and carcinogenic properties, poses a significant threat to both human health and the ecological environment [4]. Chromium, once it enters the soil, can be easily absorbed by crops and plants, creating a potential hazard to human health through the food chain [5]. This has led to numerous research efforts focusing on the effective remediation of soils contaminated with chromium.

In modern sectors such as the chemical, steel, and leather industries, chromium and its derivatives feature prominently. This usage has converted chromium pollution in groundwater, surface water, and soil into a pressing environmental matter. According to the United States Environmental Protection Agency (USEPA), chromium is among the most harmful pollutants. It primarily manifests in two forms in nature: Cr(VI) and Cr(III), with Cr(VI) being 100 times more mobile and toxic than Cr(III). Given the rapid proliferation of the chemical industry in recent times, a vast volume of chromium-laden wastewater and waste by-products have been expelled into the environment, causing serious chromium contamination of soil, groundwater, and surface water. Notably, Cr(VI), with its high water-solubility, potent oxidative properties, and carcinogenicity, poses a grave risk to both the ecological environment and human health [6]. When introduced into the soil, chromium can be readily absorbed by plants and crops via the food chain, thereby posing a risk to human health. Thus, numerous studies have concentrated efforts on devising efficient strategies for the remediation of Cr-contaminated soils [7].

In recent years, cost-effective clay minerals have gained popularity as passivation agents [8]. Layered double hydroxides (LDHs), a form of affordable and diverse clay minerals, have become increasingly utilized for the immobilization of various metals in soil [9–11]. The chemical composition of LDHs is $[M(II)_{1-x}M(III)_x(OH)_2]^{x+}(A^{n-})$ $x/n{\cdot}mH_2O$, in which M(II) and M(III) denote the divalent and trivalent metal cations found respectively on the primary laminate [12].

Due to the unique advantages, more and more researchers are applying LDHs in soil remediation. In 2018, He et al. found out that the Cr(VI) in the soil could be immobilized and reduced by Fe–Al-LDHs [13]. Huang et al. using LDHs for different heavy metals remvoal in the soil and proved that the adsorption capacities of heavy metals with the presence of microplastics are more obvious

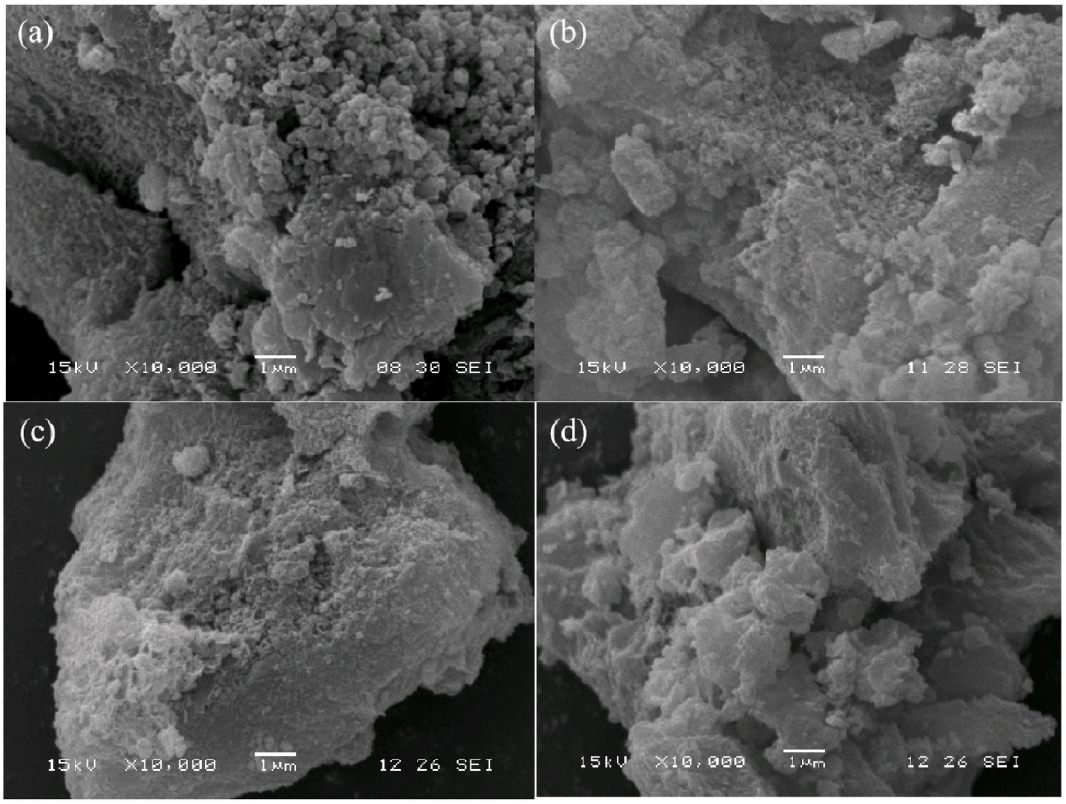

Fig. 1. SEM images of (a) LDH-D, (b) LDH-D-300, (c) LDH-D-500, and (d) LDH-D-900 before reaction.

microplastics [14]. Also, Liu et al. reported synthesized CaFe-layered double hydroxide can provide various active sites for the simultaneous removal of Cd^{2+}, AsO^{2-}, and Pb^{2+} with high removal efficiencies within 60 min [15].

Various techniques have been employed in the preparation of LDHs [16]. The main precursors in LDH synthesis are divalent and trivalent metal ions or metal oxides. In an effort to reduce costs, materials such as dolomite, magnesite, oxides, as well as magnesium and aluminium hydroxides, have been primarily used as affordable alternatives to expensive chemical reagents [17]. Dolomite, due to its global accessibility and economical price, is a strong contender. Post calcination, dolomite yields a certain quantity of MgO which can be harnessed as a foundational magnesium source in LDH synthesis [18]. By taking advantage of dolomite as a divalent metal source, LDHs have recently been engineered and efficaciously utilized for anion adsorption in various solutions [19].

Alongside this, calcination emerges as a generally applied method aimed at enhancing the adsorption efficiency of LDHs. Findings have shown that after calcination, LDHs display a significantly amplified adsorption capacity for pollutants compared to the counterparts that have not undergone calcination [20]. This is predominantly attributed to the structural memory effect [21]. Furthermore, LDHs calcined at different temperatures show diverse adsorption mechanisms, regardless of the calcination temperature exceeding that necessary for the structural memory effect [22]. Despite these advancements, there is a dearth of studies exploring the application of calcined LDHs, derived from dolomite, for treating heavy metals in contaminated soil.

This work scrutinizes the impacts of various calcination temperatures on LDHs derived from dolomite, specifically focusing on the immobilization of Cr(VI) in contaminated soils. Different influences on the immobilization performance of LDHs were studied and the immobilization mechanism linked to LDHs calcined at diverse temperatures is scrutinized. Lastly, the post-remediation leachability of Cr(VI) from the soil, its subsequent accumulation in plants, and its potential effects on the native soil microorganisms are explored.

2. Methods

The detail methods can be found in the support information. All experiments were carried out three times, and the average value was shown in the figures. The properties of the soil have been added into the support information in Table S1 and Fig. S1. Leaching of Cr from the artificially contaminated soil was also supplied in Table S2.

3. Results and discussion

3.1. Characterizations

Fig. 1 shows SEM images of uncalcined LDH-D as well as LDH-D calcined at 300 °C, 500 °C, and 900 °C. Before calcination, Fig. 1a reveals the presence of square and sheet structures on the surface. Upon calcination at varying temperatures, these hexagonal sheets have been thoroughly damaged, resulting in a coarse surface riddled with small particles due to high-temperature decomposition of the structure (see Fig. 1b–d). Fig. 2 exhibits the FTIR spectra of LDH-D, both pre- and post-calcination. Vibration peaks emerging in the 3300–3500 cm^{-1} range are accredited to the *O*–H stretching involving hydrogen bonds [23]. Peaks at 1620 cm^{-1} arise from bending vibrations of interlayer water molecules [24]. Intensity of these peaks dwindles as the calcination temperature escalates, signaling the gradual evaporation of water molecules (interlayer and surface) from LDH-D. Remarkably, uncalcined LDH-D bears a sharp

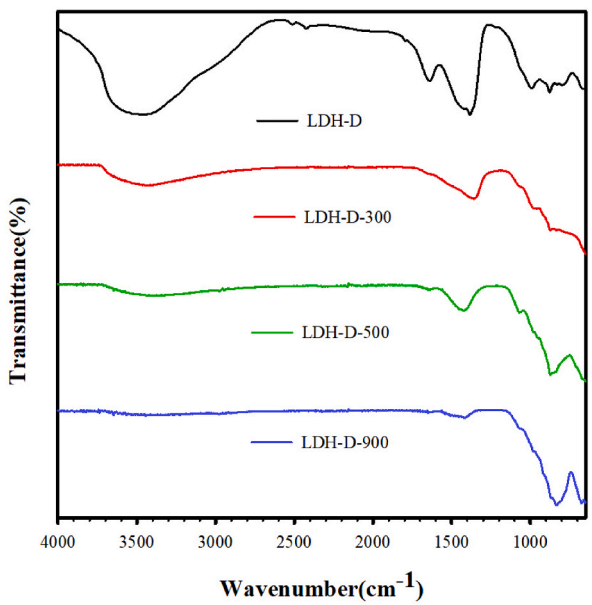

Fig. 2. FTIR spectra of (a) LDH-D, (b) LDH-D-300, (c) LDH-D-500, and (d) LDH-D-900 before reaction.

characteristic absorption peak at 1356 cm^{-1}, attributable to the C–O bond vibration of CO_3^{2-}. After calcination, this along with another peak significantly weakens due to the disapperance of the interlayer anion [25]. Peaks falling within the range of 500–800 cm^{-1} majorly signify lattice vibrations of the M − O bond (where M = Mg, Ca, Al). The absorption peak at 787 cm^{-1}, attributed to Al–OH, gradually transforms into Mg–O, Ca–O, and Al–O as the calcination temperature increases [26].

Fig. 3 exhibits the XRD patterns for LDH-D and calcined at diverse temperatures. Prior to calcination, the XRD pattern of LDH-D reveals peaks at 11.45° (003) and 23.29° (006). These can be credited to the formation of Mg–Al-LDH, displaying a layer spacing of about 7.8 Å [27]. Since the interlayer of CO_3^{2-} rests at approximately 7.65 Å [28], it can be deduced that the predominant anion in LDH-D is primarily CO_3^{2-}. Besides the LDHs, the pattern also highlights the presence of $CaCO_3$, courtesy of the observed peaks at 29.87°, 40.02°, and 49.31° [29]. Moreover, by using the Maud software, the weight contents of $CaCO_3$ in the LDH-D were found to be 77.6 % [30]. Due to the loss of interlayer water during calcination at 300 °C, the peaks, which include (003) and (006), became broader. With calcination at 500 °C, the (003) and (006) peaks linked to MgAl-LDH vanish, while new peaks surface at 43.42°, which are characteristic indicators of MgO [31]. This suggests a collapse of the LDHs structure, prompted by the significant loss of water molecules and the CO_3^{2-} interlayer anion. Additionally, the freshly-emerged MgO peaks are broader, denoting their amorphous bimetallic oxide nature and the partial replacement of Mg^{2+} ions in MgO by Al^{3+} ions. Upon elevating the temperature to 900 °C, CaCO3 undergoes decarbonation, and the peak of MgO sharpens due to the formation of spinel [17].

3.2. Influence of the calcination temperature on the immobilization of Cr in the soil

In Fig. 4, without any form of treatment, the soil leached out 63.17 mg/L of Cr(VI). After the added of LDH-D into the soil, the immobilization efficiency plateaued at around 45.19 % post 48 h. At a calcination temperature of 300 °C, the immobilization efficiency was 46.46 %, which nearly paralleled the efficiency of the un-calcinated one. This could be attributed to the fact that at this specific calcination temperature, the only changes in the LDHs compared to the calcined material pertained to adsorbed water, while their fundamental structure stayed intact. The most pronounced boost in immobilization was observed at 500 °C, with an efficiency of 62.82 % for Cr(VI) in the first 6 h of the reaction time, which then escalated to 85.05 % at the 48 h. This could be due to the disappearance of both water and anions in the interlayer of the LDHs, the collapse of the lamellar structure, and exposure of adsorption sites after calcination at 500 °C. Moreover, when calcined at this temperature, the bimetallic oxides born from the calcination of LDHs exhibited a structure memory effect, enabling the reversion of the structure to a layered state during immobilization, leading to high immobilization efficiency. Nevertheless, the adsorption efficiency decreased as the calcination temperature was elevated to 900 °C. After 48 h of reaction, the immobilization efficiency for Cr in the soil was merely 30.01 %. Upon calcination at 900 °C, the material morphed into a spinel structure, which was unable to revert to its original layered structure, rendering its Cr adsorption significantly less effective.

3.3. Influence of the dosage on the remediation performance

Fig. 5 (a-d) illustrates the leachability of Cr(VI) in soil post-treatment using both calcined and uncalcined LDH-D. As time evolved and with various dosages, LDH-D's ability to confine Cr(VI) heightened. Among all the materials tested under equal dosage, LDH-D-500, which was calcined at 500 °C, demonstrated a superior immobilization efficacy for Cr(VI) in soil. This finding aligns well with the previously discovered patterns. In an instance with a dosage of 0.03 g, this material achieved an immobilization rate of 85.05 % at the

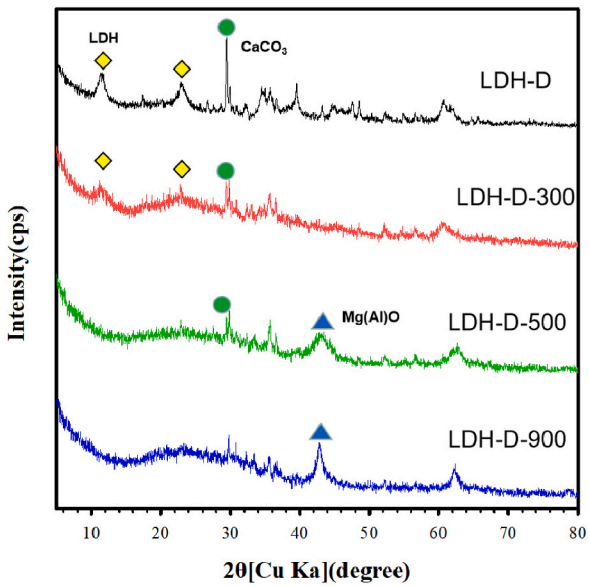

Fig. 3. XRD patterns of (a) LDH-D, (b) LDH-D-300, (c) LDH-D-500, and (d) LDH-D-900.

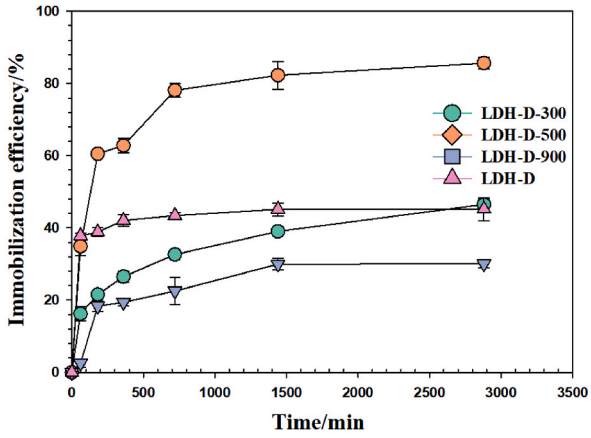

Fig. 4. Immobilization efficiency of LDH-D calcined at different temperatures for Cr-containing soils with a dosage of 0.03 g, initial Cr concentration of 600 mg/kg.

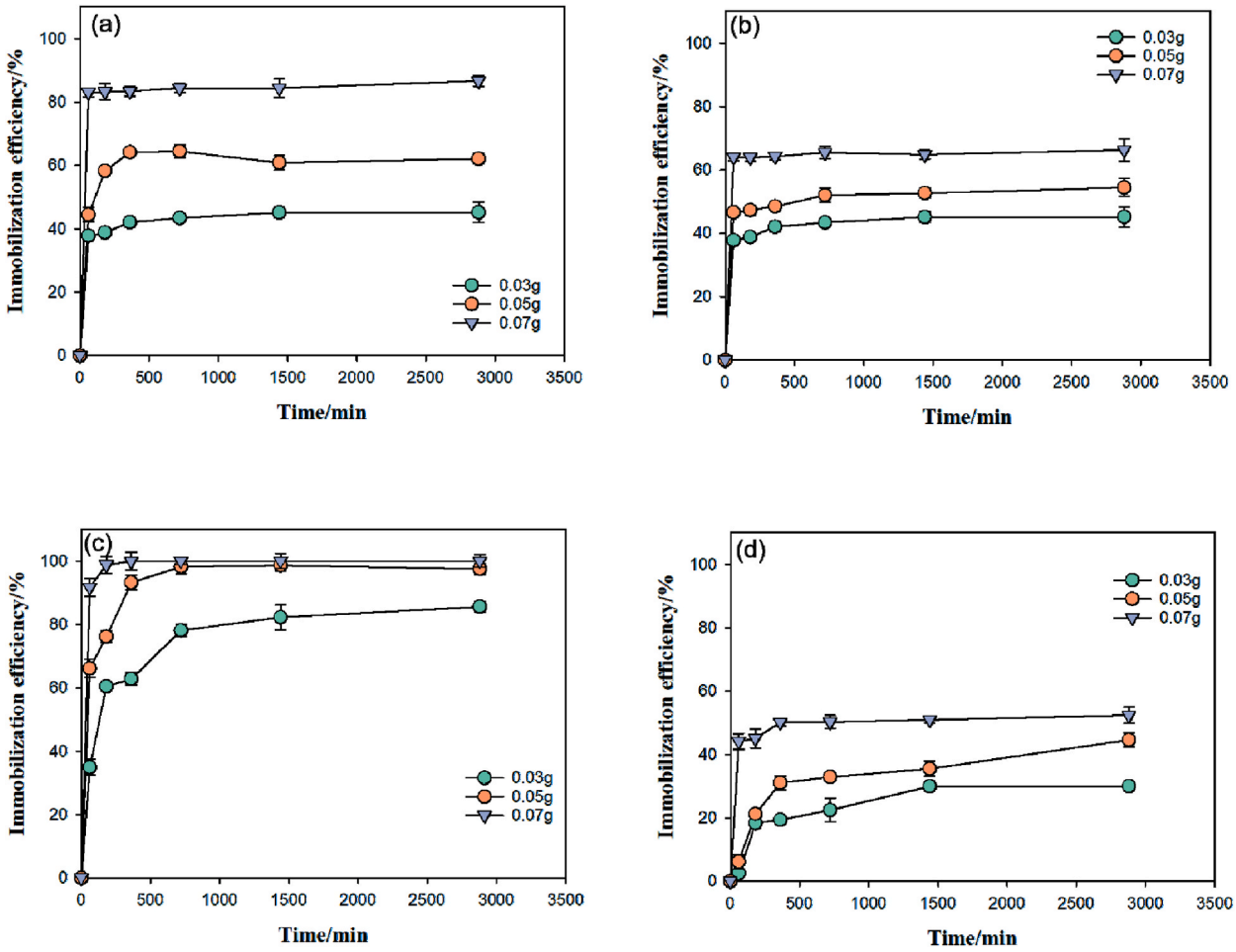

Fig. 5. Immobilization efficiency of LDH-D calcination at different temperatures for Cr-containing soils with different dosages: (a) LDH-D, (b) LDH-D-300, (c) LDH-D-500, and (d) LDH-D-900 (initial Cr concentration of 600 mg/kg in soil).

48-h mark. Furthermore, the efficiency for Cr(VI) in soil ascended to 100 % upon augmenting the dosage to 0.07 g, merely 6 h after the addition. An up-tick in curing efficiency is attributable to the expansion of adsorption sites resultant from dosage increase. Also worth noting, the material calcined at 300 °C had an immobilization rate practically indistinguishable from that of the non-calcined sample

across distinct dosages [32]. At an application rate of 0.03 g, both materials exhibited an immobilization efficiency for Cr of 46.46 %. Further elevation of the dosage led to a substantial upswing in the efficiency, peaking at 66.30 % at a usage level of 0.07 g. Consistent with prior results, the sample calcined at 900 °C manifested the most inferior immobilization, with an efficiency meriting a mere 52.38 % when the dosage was boosted to 0.07 g.

3.4. Influence of initial concentration on remediation performance

Fig. 6 illustrates how the initial Cr(VI) concentration in the soil influences the effectiveness of Cr(VI) immobilization. As the Cr concentration in soil escalated from 400 to 1000 mg/kg, there was a noticeable decline in the efficacy of LDH-D immobilization. For non-calcined samples, immobilization efficiency depreciated to 52.86 %, eventually sinking to 19.04 %. Meanwhile, the immobilization efficiency of the material calcined at 500 °C dwindled from 97.08 % to a moderate 66.62 %. A plausible explanation for these diminishing trends could be the deficiency in binding sites [33].

3.5. Impact of initial pH on remediation performance

According to Fig. 7, at a pH of 3, LDH-D and LDH-300 demonstrated almost identical Cr immobilization efficiencies, with 28.21 % and 28.07 % respectively. LDH-D-500 exhibited an astonishing efficiency of 92.52 %, whereas LDH-D-900 maintained the lowest efficacy, delivering a meager 16.37 %. The immobilization efficiency generally decreased when the pH was 10. To illustrate, the efficiency of LDH-D dropped to 23.65 %, and that of LDH-D-500 stood at 89.21 %. The declining efficiency under alkaline conditions can be attributed to the antagonism from OH^- ions that occupied the adsorption site in the interlayer [29].

3.6. TCLP leaching results

The TCLP leaching tests were widely utilized to assess the effectiveness of the method used to immobilize toxic metals in contaminated soils [22]. Fig. 8 presents the highest amount of Cr (32.34 mg/L) leached from untreated soil. After treatment, there was a decrease in Cr leaching in the soils where different LDHs initiated fixation, implying that Cr can be immobilized in the soil by LDH-D at different calcination temperatures. Cr(VI) leaching from soils treated with LDH-D, LDH-D-300, LDH-D-500, and LDH-D-900 was 22.32 mg/L, 21.01 mg/L, 16.16 mg/L, and 24.21 mg/L respectively at 0.03 g. When the dose was increased to 0.07 g, the Cr leaching from soil dropped to 13.72 mg/L, 12.62 mg/L, 6.659 mg/L, and 15.262 mg/L after a 48 h reaction. These findings showed that LDH-D, especially at a 500 °C calcination temperatureand, could immobilize Cr in soil and were relatively stable.

3.7. Cr(VI)-containing soil phytotoxicity tests

At the commencement of the incubation phase, all the mung beans germinated successfully (Fig. 9). Nevertheless, as the incubation period extended, only a small fraction of the beans fully developed roots and leaves. At the end of this phase, the pure soil showcased the best growth, achieving a 100 % survival rate. Extremely toxic Cr(VI) led to a mere 13.33 % survival rate of mung beans in the untreated soil contaminated with Cr. On treating the soil with LDH-D-500, the growth of mung beans improved significantly with a survival rate reaching 100 % (Table 1). An observable growth in roots, stems, and leaves was also noted (Fig. 10 and Table 2). LDH-D-500 effectively reduced the Cr content in the plant without adversely affecting the growth of mung beans. Root, stem, and leaf lengths of mung bean seedlings treated with LDH-D-500 expanded to 31.14, 65.07, and 16.14 mm, respectively, compared to the control during germination. Mung bean seeds treated with LDH-D-500 demonstrated better growth than contaminated samples. Table 2

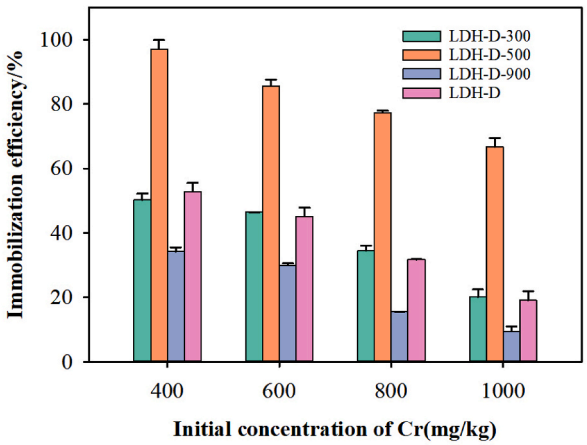

Fig. 6. Immobilization efficiency of LDH-D and for Cr-containing soils with different Cr concentrations, with a loading for Cr of 0.03 g/g, 1 g of soil and a shaking time for Cr immobilization of 2880 min.

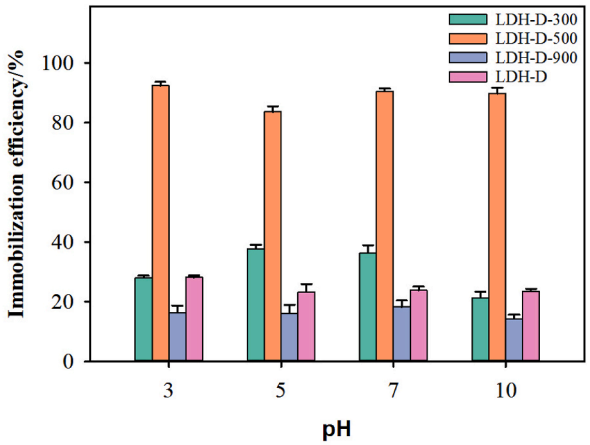

Fig. 7. Influence of the initial pH on the immobilization efficiency of Cr by LDH-D for different calcined temperatures, with a loading for Cr of 0.03 g/g, 1 g of soil and a shaking time for Cr immobilization of 2880 min.

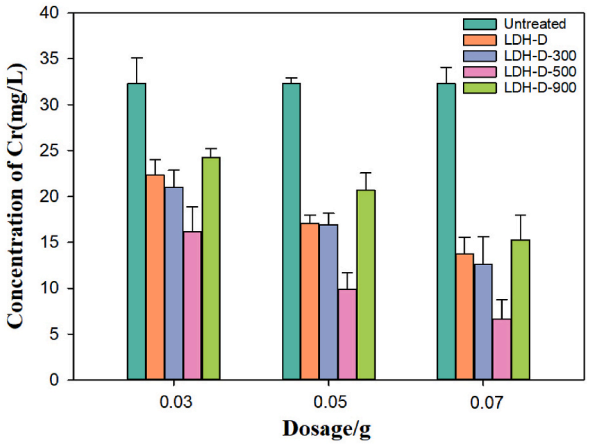

Fig. 8. TCLP leachability of Cr before and after the soil samples were treated, with an initial Cr concentration of 600 mg/kg, 1 g of soil and a shaking time for Cr immobilization of 2880 min.

showcased the biomass of mung beans cultivated in various soil types. Although lower than that of the minimally contaminated samples, the biomass of plants treated with LDH-D-500 increased compared to the contaminated samples. Table 3 depicted the total Cr content within plant tissues. The plant tissues from uncontaminated soil had the lowest overall Cr concentration. The Cr(VI) content in mung beans under diverse conditions was examined. It was found that LDH-D-500 treatment managed to considerably reduce the Cr (VI) content in all parts of the mung beans. This established that LDH-D-500 effectively removed Cr(VI) from chromium-contaminated soil and obstructed Cr(VI) uptake by plants.

3.8. Soil microbial community after treatment in different time

To determine the effect of LDHs-M on soil microbiota, we employed Illumina MiSeq platform for 16 S rRNA gene sequencing to analyze microbial diversity over time. Table 4 illustrates the changes in OTU number and community diversity index of soil microorganisms following the application of LDH-D-500 passivator to chromium-contaminated soil across varying incubation periods. The high-throughput sequencing coverage for each treatment exceeded 99 %, indicating robust detection of species within the samples. Overall, differences in incubation time were found to impact the diversity of soil microbial communities, with the application of this passivator consistently leading to increased community diversity indices with prolonged incubation. The Chao1 and ACE indices are indicative of the actual number of species present in the microbial community, with higher values suggesting greater community richness. Meanwhile, Simpson's index is more sensitive to the community's evenness and the dominance of specific OTUs. Regarding microbial community richness, both the ACE and Chao1 indices of soils treated with this passivator increased with prolonged incubation, indicating subsequent enhancement of microbial community richness. In terms of microbial community diversity, the Shannon index demonstrated an increase with prolonged incubation following the application of LDH-D-500, peaking after one month with the

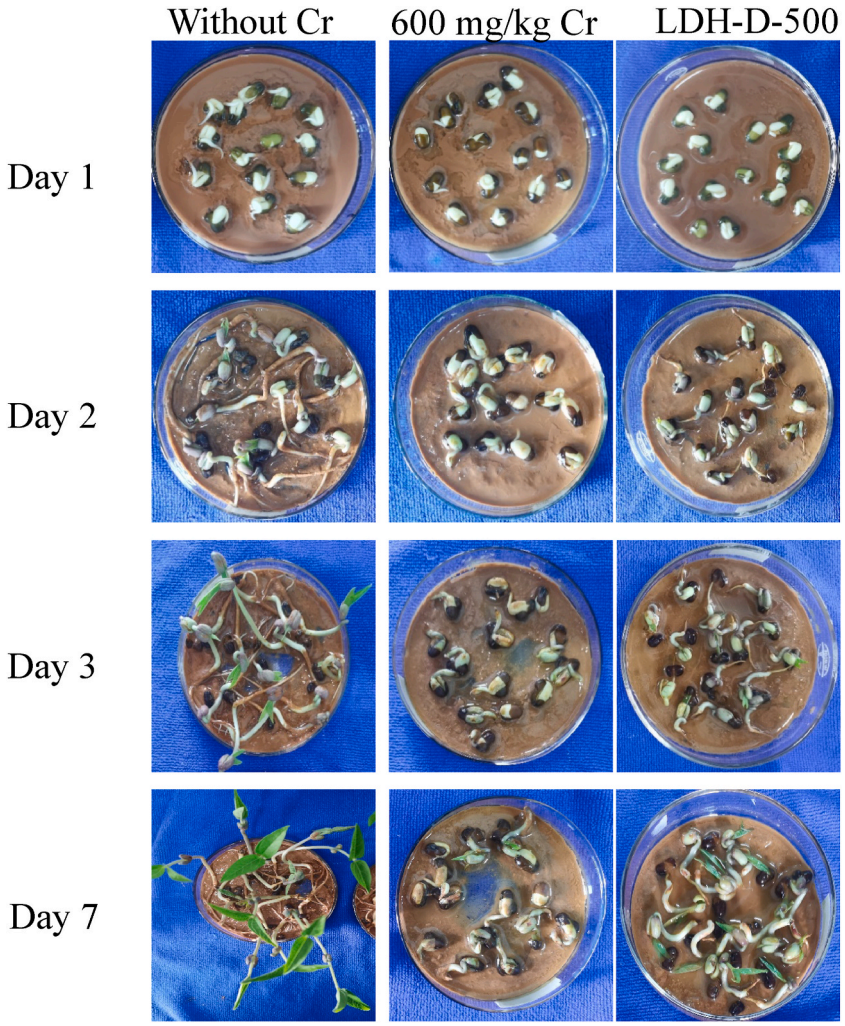

Fig. 9. Photographs of the cultivation process of plants in different soil samples for one week.

Table 1
Survival rate of seeds in differently treated soil[a].

	Clean soil	Contaminated soil	Treated with LDH-D-500
Mung beans	100 %	30 %	100 %

[a] The results are calculated based on the number of survivals.

highest community diversity observed. Thus, it can be speculated that extending the incubation time may augment both the richness and homogeneity of microbial communities. Furthermore, the Rarefaction curve (Fig. 11) for various incubation times subsequent to the application of the two passivators all plateaued as the number of sequences increased, suggesting that the number of OTUs was adequate to represent the diversity of the current samples.

The relative abundance analysis (Fig. 12) revealed that the dominant phyla in the LDH-D-500 treated group after various incubation periods included Actinobacteria, Proteobacteria, Chloroflexi, and Acidobacteria, collectively constituting relative abundances ranging from 80.74 % to 82.94 %. Notably, Actinobacteria and Ascomycetes exhibited the most pronounced changes in relative abundance, while Chloroflexi and Acidobacteria remained relatively stable. The relative abundance of the Actinobacteria phylum gradually increased from 33.87 % to 43.06 % with prolonged incubation time. Studies have demonstrated a significant negative correlation between the Actinobacteria phylum and the total amount of heavy metals. Actinobacteria are frequently found in soils contaminated with heavy metals, and this group can supplant more vulnerable fungi as the primary decomposers in soil [34]. Furthermore, their relative abundance tends to increase with decreasing pollutant concentrations. Thus, we speculate that extending the incubation time may also lead to a reduction in the concentration of Cr(VI) in the soil. Conversely, the relative abundance of

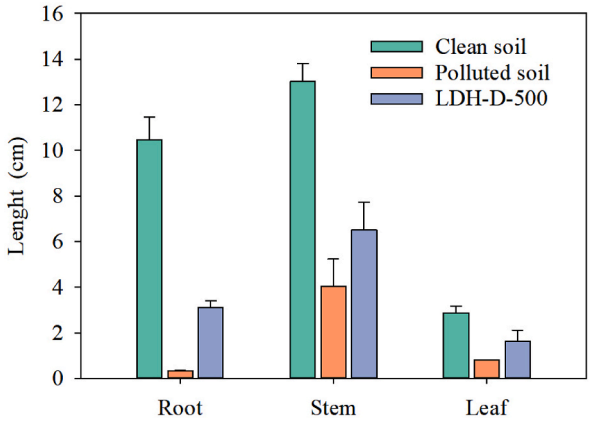

Fig. 10. Length of roots, stems, and leaves of plants grown in different soil samples after one week.

Table 2
Dry biomass of the seeding grown in differently treated soils. Note that the results are calculated in mg.

Mung bean (mg)	Free soil	Polluted soil	LDH-D-500
Root	7.01 ± 0.29	2.61 ± 0.33	5.28 ± 0.15
Stem	23.22 ± 0.95	8.12 ± 0.89	18.74 ± 0.53
Leaf	7.25 ± 0.35	0.74 ± 0.27	5.13 ± 0.57

Table 3
Cr distribution in root, stem, and leaf of plants grown in different Cr(VI)-containing soil samples. Note that the results are calculated in mg of Cr per g of dry plant tissue.

Mung bean (mg/g)	Free soil	Polluted soil	LDH-D-500
Root	0.55 ± 0.02	177.70 ± 6.08	27.11 ± 2.28
Stem	0.49 ± 0.11	41.78 ± 2.29	67.26 ± 2.73
Leaf	0.43 ± 0.06	245.69 ± 3.33	19.59 ± 1.94

Table 4
Soil Microbial Community Diversity after treatment with LDH-D-500 in different times.

Time	Coverage %	OTUs	ACE	Chao1	Shannon
CaAl-500°C-1D	99.78	870	870.21	897.10	5.51
CaAl-500°C–1W	99.85	978	991.89	1033.37	5.57
CaAl-500°C–2W	99.56	1028	1060.22	1098	5.60
CaAl-500°C-1M	99.83	1160	1172.77	1191.03	5.68

Ascomycota exhibited a declining trend with prolonged incubation time, decreasing from 33.26 % to 26.82 %. Previous research has shown the presence of robust metal resistance genes in Ascomycetes and Thickettsia [35], aligning with our findings and providing a rationale for the decreased abundance of Ascomycetes and Thickettsia with decreasing heavy metal concentrations. In some studies, it was observed that uncontaminated or less contaminated sites exhibited similar phylum-level characteristics, with Actinobacteria, Aspergillus, and Green Bay phylum being the most abundant phyla present [36–38]. Similar findings were corroborated in the current study. Additionally, Gemmatimonadetes, Myxococcota, and Thermoproteota were present in all soils, albeit with low relative abundance and no significant fluctuations in the relative abundance of other bacterial phyla.

The results of PCoA analysis are depicted in Fig. 13. The closer the proximity of sample points in the PCoA analysis plot representing the microbial community of soil samples, the more similar the community structure. In the LDH-D-500 treatment group, the contribution of the first principal component (PCoA1) to sample variation was 42.26 %, while the second principal component (PCoA2) contributed 31.04 %, indicating that different incubation times influenced the structure of the soil microbial community. Samples subjected to 1 and 2 weeks of incubation exhibited closer proximity, suggesting a similarity in microbial community structure between these two treatment groups. The abundance heatmap of species serves to visually represent the differences in abundance between communities. A redder color indicates greater abundance, signifying a larger disparity between communities, while a bluer color suggests lower abundance. Soil microorganism species abundance at the genus level was examined following incubation of LDH-D-500 remediated soil for various durations. The top 50 species, based on total abundance, were selected, plotted on heatmap diagrams, and

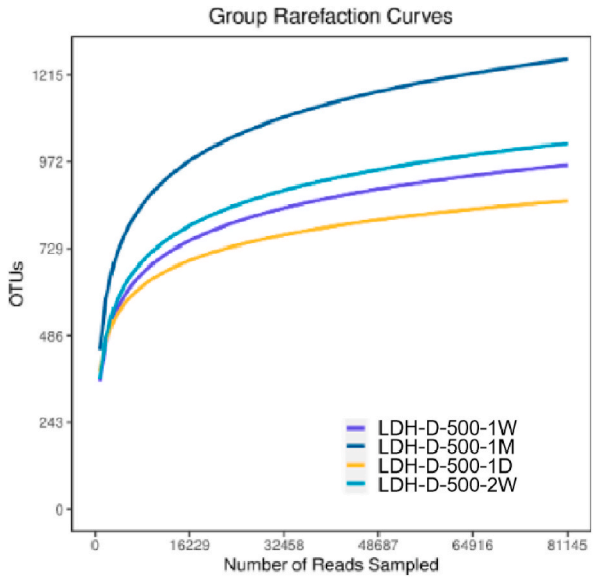

Fig. 11. Rarefaction curve analysis of diversity index for all groups (Treat with LDH-D-500 after one day (1D), one week (1 W), two weeks (2 W) and one month (1 M)).

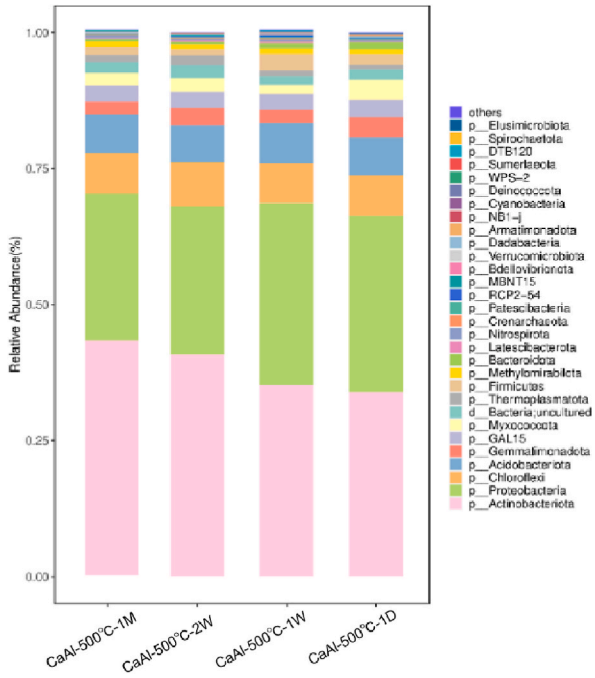

Fig. 12. The relative abundance of bacterial species in soil at phylum level.(Treat with LDH-D-500 after one day (1D), one week (1 W), two weeks (2 W) and one month (1 M)).

subjected to clustering analysis. The results are illustrated in Fig. 14. The relative abundance of Nocardioides, IMCC26256, Lysobacter, and Acidimicrobiia significantly increased with prolonged incubation time, with the highest relative abundance of Nocardioides and IMCC26256 strains observed after one month of incubation. This suggests that these microorganisms exhibit high resistance to heavy metals [39]. Conversely, the relative abundance of other flora was lower and not significantly different.

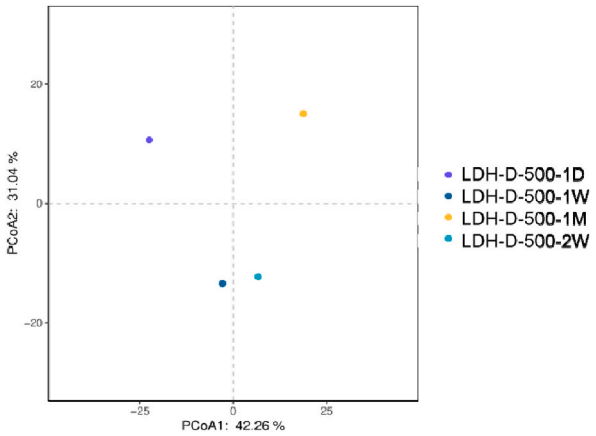

Fig. 13. PCoA analysis of microbial communities (Treat with LDH-D-500 after one day (1D), one week (1 W), two weeks (2 W) and one month (1 M)).

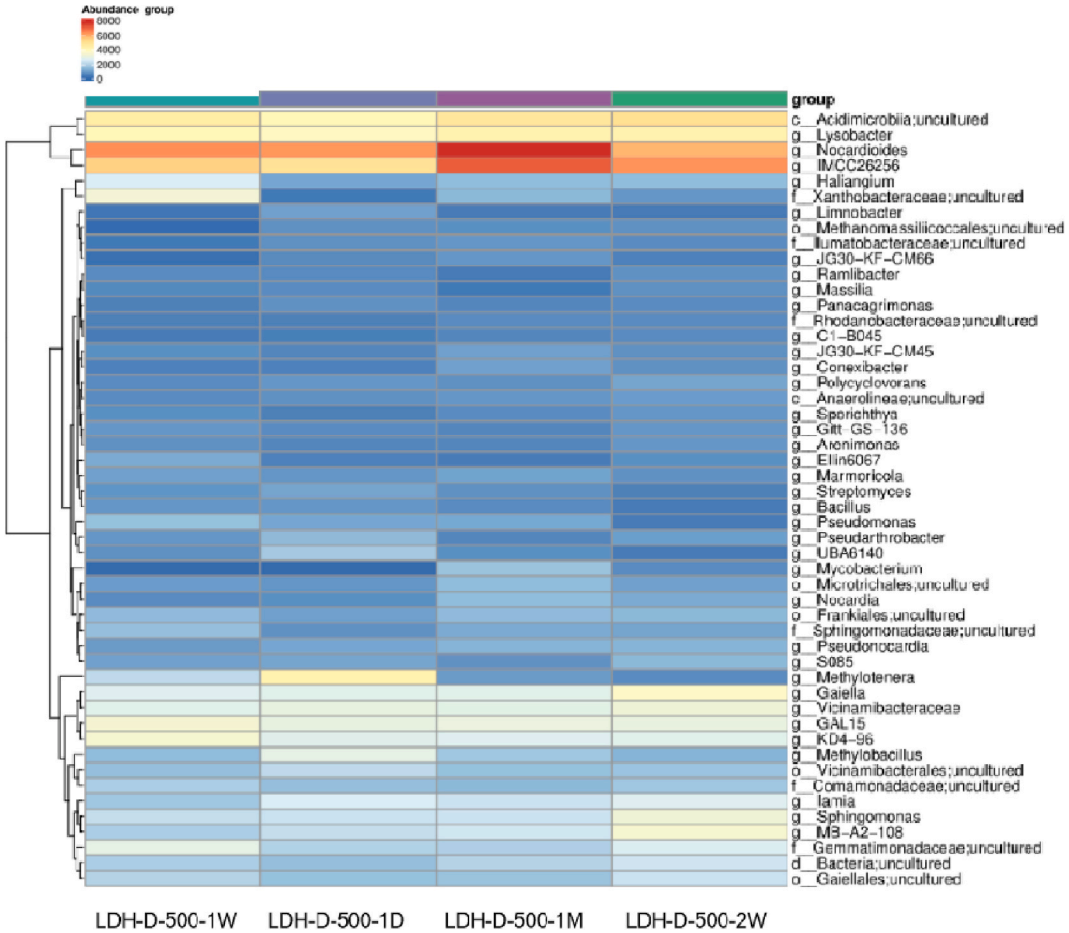

Fig. 14. Heat map of sample average abundance (Treat with LDH-D-500 after one day (1D), one week (1 W), two weeks (2 W) and one month (1 M)).

3.9. Mechanism analysis

Considering that LDH-D and its calcined products were in powder form, it posed a significant challenge in sample collection. In order to delve into the precise reaction mechanism, we applied the soil solution method. The sample was subjected to a reaction process within a soil solution, followed by the use of SEM, XRD, and XPS to unravel the mechanism behind the passivation of Cr(VI) in the soil.

Fig. 15 displays the SEM images of different materials following their reaction. This figure reveals that the morphological transformations of LDH-D (Fig. 15a) and LDH-D-300 (Fig. 15b) due to adsorption are negligible, in contrast to LDH-D-500, which exhibited notable morphological changes characterized by the emergence of a lamellar structure. This suggests that the original oxides in LDH-D-500 (Fig. 15c) were converted into a lamellar configuration prior to calcination as a result of the reaction. The principal structure in LDH-D-900 (Fig. 15d) is that of a spinel, thus the adsorption process did not markedly alter its morphology. Fig. 16 presents the XRD spectra of LDH-D and LDH-D-300 after immobilization. It is observed that their XRD characteristic peaks remain virtually unchanged, signifying that the layered composition of LDHs is preserved during adsorption. Conversely, the XRD pattern of LDH-D-500 post-reaction shows alterations, with the explicit emergence of LDH characteristic diffraction peaks, and a reduction in the intensity of the peak linked to Mg(Al)O. This demonstrates that structure of LDH-D-500 shifts back towards its original layered organization post-reaction, with an interlayer distance approximately at 7.8 nm. However, diffraction peaks in LDH-D-900 remain unaltered post-Cr (VI) adsorption, indicating the retention of its primary spinel structure. Following an analysis based on these characterization outcomes and existing literature [21,22], the mechanism through which LDH-D and its calcined derivatives remediate Cr(VI) in soil was explained. Given that the structures of LDH-D and LDH-D-300 were preserved after reaction, their adsorption of Cr(VI) primarily occurs through interlayer anion exchange and surface adsorption. On the other hand, LDH-D-500 demonstrates a structural memory effect. As it reverts to its initial layered structure, CrO_4^{2-} and CO_3^{2-} are drawn into the interlayers via electrostatic attraction, while the remainder adhere to the surface. Lastly, LDH-D-900, being predominantly $MgAl_2O_4$, undergoes no structural changes after reacting. Consequently, its Cr(VI) adsorption mainly stems from surface adsorption and electrostatic attraction.

However, ion exchange may not be the primary means of adsorption. Before the reaction, the XRD pattern shows characteristic diffraction peaks of LDH-D at 11.45° (003), 23.29° (006), and 35.51° (009), indicating the formation of Mg–Al-LDH with an interlayer spacing of 7.8 Å. Typically, the interlayer spacing of NO_3^- is greater than 8.0 Å, while that of CO_3^{2-} is around 7.6 Å, suggesting that carbonate ions have entered the interlayer space, making CO_3^{2-} the predominant anion in LDH-D [40]. The molar ratios of LDHs were analyzed using CHN analysis and flame atomic absorption spectroscopy. Based on previous report [21], the molar ratios and formulae of LDH were determined to be $Mg_{0.73}Al_{0.33}(OH)_2(NO_3^-)_{0.03}(CO_3^{2-})_{0.21}\cdot nH_2O$, indicating that less nitrate ions remained in the interlayer.

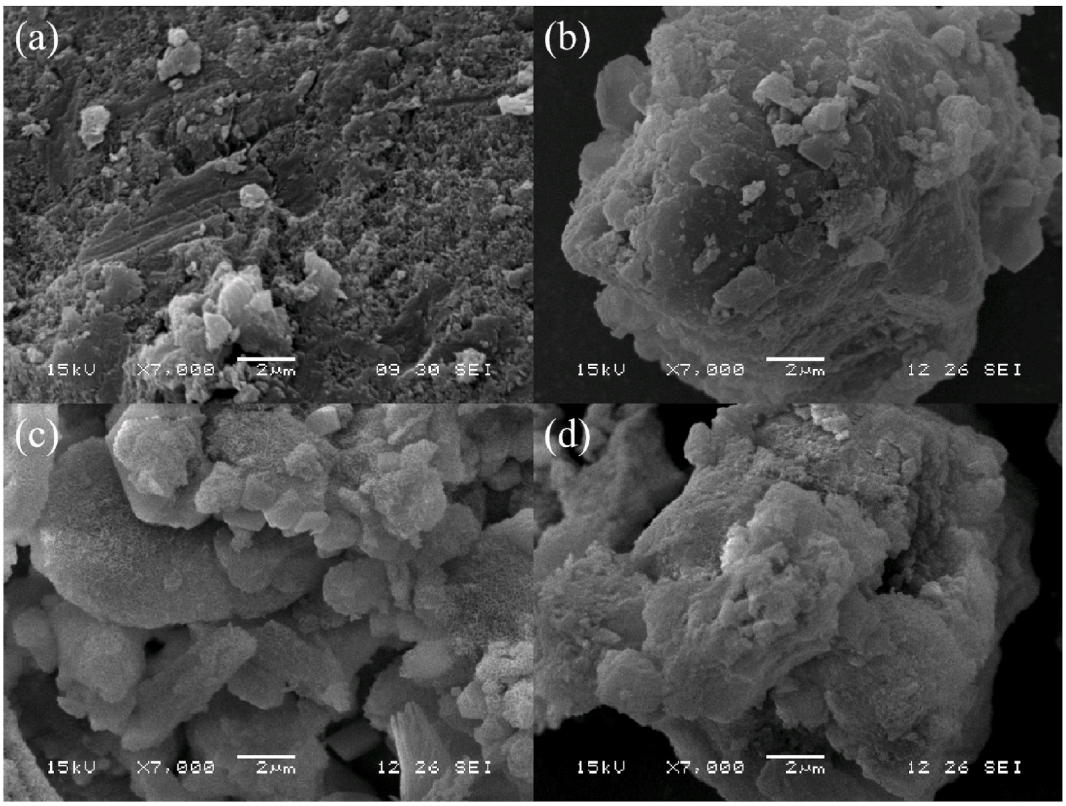

Fig. 15. SEM images of (a) LDH-D, (b) LDH-D-300, (c) LDH-D-500, and (d) LDH-D-900 after reaction.

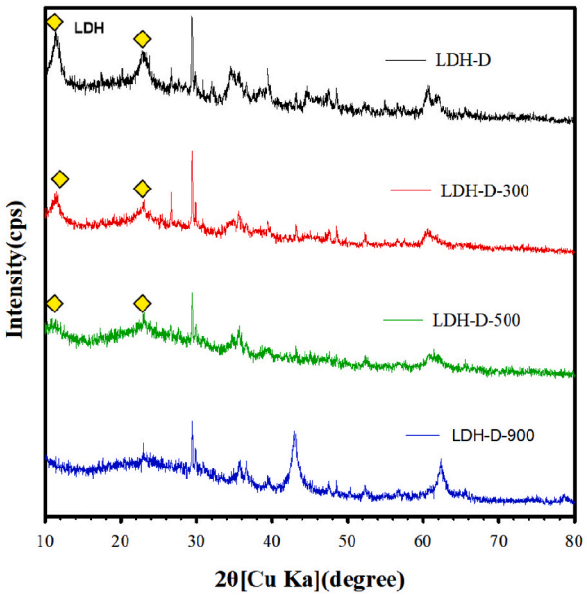

Fig. 16. XRD patterns of (a) LDH-D, (b) LDH-D-300, (c) LDH-D-500, and (d) LDH-D-900 after reaction.

Calcination at 300 °C also resulted in a layer spacing of 7.8 Å, but calcination at 500 °C and 900 °C caused the layer structure to disappear. After adsorption, the layer spacing of both LDH-D and LDH-D-300 became 7.7 Å, likely due to a small amount of NO_3^- being exchanged by heavy metals. However, ion exchange may not be the main mode of adsorption due to the presence of carbonate.

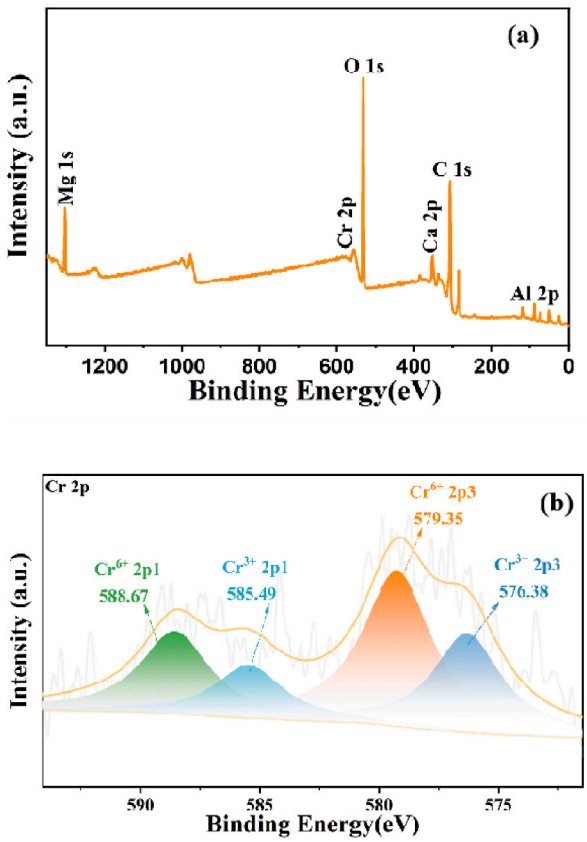

Fig. 17. XPS spectra of LDH-D-500 after the reaction(a) XPS surveys; (b)narrows scan of Cr(VI).

Meanwhile, the interlayer spacing of the regenerated LDH-D-500 was also 7.8 Å, suggesting that some CO_3^{2-} from the soil entered the interlayer during the remediation process. Therefore, while ion exchange exists in this process, it is not the primary mechanism. In addition, it can be seen that all the samples contain $CaCO_3$ (Fig. 16), so $CaCO_3$ should have an important role in the adsorption process. According to the reports [41,42], it is suggested that Cr(VI) can be adsorbed by the surface of $CaCO_3$. So, $CaCO_3$ was play an important role in the immobilization.

In addition, an XPS study was conducted on the high-performance LDH-D-500, and the findings are illustrated in Fig. 17. The XPS surveys showed that Mg, Al, Ca, and Cr metal elements were present in LDH-D-500 post-reaction (Fig. 17a). Following immobilization, Cr2p scanning was performed (Fig. 17b). The characteristic binding energy peaks at 579 eV and 588 eV are attributed to Cr(VI), while those located at 576eV and 585 eV correspond to Cr(III) [43]. It was observed that adsorbed Cr(VI) in the solid was partially reduced to Cr(III). As found by Li et al. [44], the reduction of Cr(V579 eV and 588 eV are attributed to Cr(VI), while those located at 576eV and 585 eVI) anions to Cr(III) cations occurs due to electron provision by abundant LDH hydroxyl groups. Under standard conditions, Cr (VI) is easily reduced to Cr(III) in acidic media owing to its high redox potential. Additionally, due to the close ionic radius of Cr(III) and Al(III), some of the Al(III) on LDH laminates could be replaced by Cr(III). The adsorption mechanism of Cr by materials of varying calcination temperatures is summarized in Fig. 18.

4. Conclusion

In this work, we prepared LDH-D based on dolomite, and calcined it at 300 °C, 500 °C, and 900 °C. We then applied it for the immobilization study of Cr(VI) in soil. The results showed that LDH-D-500 obtained from calcination at 500 °C exhibited the best immobilization efficiency. Toxicity leaching tests revealed that Cr immobilized by LDH-D-500 was not easily leached out, further verifying the effectiveness of the material for Cr immobilization. Subsequent plant toxicity and microbial community change experiments also demonstrated that LDH-D-500 could effectively reduce the impact of Cr in the soil on plant growth and microorganisms. Finally, we discussed the material's immobilization mechanism by combining XRD and SEM. We found that LDH-D and LDH-D-300 mainly immobilized Cr(VI) through interlayer anion exchange and surface adsorption. In contrast, LDH-D-500 immobilized Cr(VI) mainly through the unique "structural memory effect" of LDHs. However, for LDH-D-900, due to its primary structure being spinel and its difficulty in structural regeneration, its adsorption performance was relatively weak. As the discussion, compare this to some conventional techniques such as $FeSO_4$ remediation, LDHs also have several key advantages in remediating Cr(VI) contaminated soil. LDHs exhibit higher efficiency in immobilization of Cr(VI) and it could reduce it into the less toxic Cr(III) through their strong anion exchange capacity and abundant active sites in their layered structure. They also provide long-term stability by forming stable Cr(III)-LDH phases, preventing re-oxidation of Cr(III) back to Cr(VI). Environmentally, LDHs are non-toxic and do not introduce secondary pollutants, unlike $FeSO_4$, which can increase soil acidity and introduce excess iron. LDHs are versatile, allowing for tailored

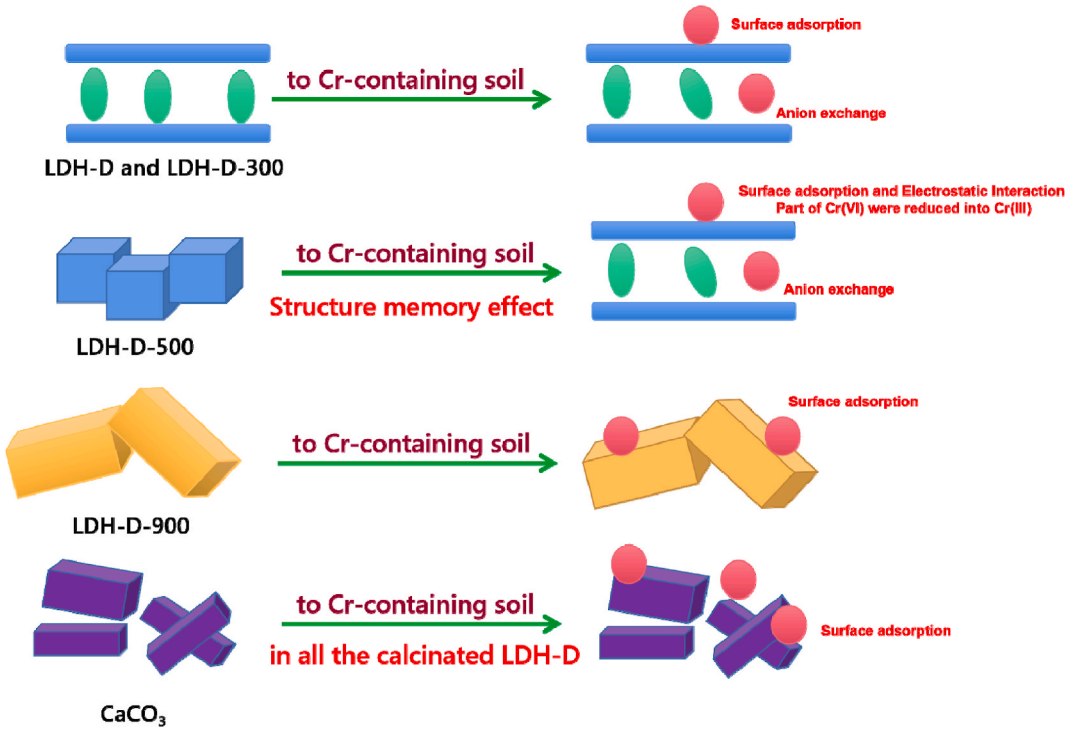

Fig. 18. Immobilization mechanism of Cr(VI) onto LDH-D, LDH-300, LDH-500, and LDH-900.

compositions to suit specific soil conditions and contaminants, enhancing their remediation efficacy. Additionally, LDHs improve soil properties by increasing buffering capacity and nutrient retention, promoting plant growth and soil health post-remediation. In contrast, $FeSO_4$ has limited flexibility and effectiveness, and any unreacted Fe^{2+} can be oxidized, reducing its long-term efficacy. Overall, LDHs offer a more efficient, stable, and environmentally friendly solution for Cr(VI) remediation in contaminated soils. The discussion has been added into the revised manuscript.

Funding

The research project was supported by Shanxi Scholarship Council of China (2021-045). Open found of Key Laboratory of Xinjiang Coal Resources Green Mining, Ministry of Education, Xinjiang Institute of Engineering (KLXGY-KA2405).

CRediT authorship contribution statement

Donghua Zhang: Writing – original draft, Resources, Conceptualization. **Zhimeng Liu:** Writing – review & editing, Visualization, Supervision, Resources, Data curation.

Declaration of competing interest

The authors declare that they have no known competing financial interests or personal relationships that could have appeared to influence the work reported in this paper.

Acknowledgment

The research project was supported by Shanxi Scholarship Council of China(2021-045). Open found of Key Laboratory of Xinjiang Coal Resources GreenMining, Ministry of Education, Xinjiang Institute of Engineering (KLXGY-KA2405).

Appendix A. Supplementary data

Supplementary data to this article can be found online at https://doi.org/10.1016/j.heliyon.2024.e34664.

References

[1] Shiv Prasad, Krishna Kumar Yadav, Sandeep Kumar, Neha Gupta, Marina MS. Cabral-Pinto, Shahabaldin Rezania, Neyara Radwan, Javed Alam, Chromium contamination and effect on environmental health and its remediation: a sustainable approaches. J, Environ. Manag. (2021) 112174.
[2] Joel Barnhart, Chromium chemistry and implications for environmental fate and toxicity, Soil Sediment Contam. (1997) 561–568.
[3] Simranjeet Singh, T.S. Sunil Kumar Naik, Vishakha Chauhan, Nabila Shehata, Harry Kaur, Daljeet Singh Dhanjal, Liliana Aguilar Marcelino, Shipra Bhati, S. Subramanian, Joginder Singh, Ecological effects, remediation, distribution, and sensing techniques of chromium, Chemosphere (2022) 135804.
[4] Amina Othmani, Sara Magdouli, P. Senthil Kumar, Ashish Kapoor, Padmanaban Velayudhaperumal Chellam, Ömür Gökkuş, Agricultural waste materials for adsorptive removal of phenols, chromium (VI) and cadmium (II) from wastewater: a review, Environ. Res. (2022) 111916.
[5] Mohammad Main Uddin, Mohamed Cassim Mohamed Zakeel, Junaida Shezmin Zavahir, Faiz Mmt Marikar, Israt Jahan, Heavy metal accumulation in rice and aquatic plants used as human food: A general review, Toxics (2021) 360.
[6] Xilu Chen, Xiaomin Li, Dandan Xu, Weichun Yang, Shaoyuan Bai, Application of nanoscale zero-valent iron in hexavalent chromium-contaminated soil: a review, Nanotechnol. Rev. (2020) 736–750.
[7] Ling Yao, Yezi Hu, Yingtong Zou, Zhuoyu Ji, Shuxian Hu, Cong Wang, Ping Zhang, Hui Yang, Zewen Shen, Duoyue Tang, Sai Zhang, Guixia Zhao, Xiangke Wang, 2022. Selective and efficient photoextraction of aqueous Cr(VI) as a solid-state polyhydroxy Cr(V) complex for environmental remediation and resource recovery, Environ. Sci. Technol. (2022) 14030–14037.
[8] Shingo Machida, Ken-Ichi Katsumata, Atsuo Yasumori, Preparation of an anion-adsorbed inorganic filter by coating of layered double hydroxide on glass-bead filter disk, Clay Sci. (2021) 1–5.
[9] Shifeng Zhao, Zhaosong Li, Haiyan Wang, Hanhan Huang, Caifeng Xia, Derui Liang, Junshan Yang, Qian Zhang, Zilin Meng, Effective removal and expedient recovery of as (V) and Cr (VI) from soil by layered double hydroxides coated waste textile, Sep. Purif. Technol. (2021) 118419.
[10] Xuanru Li, Liuwei Wang, Bei Chen, Yuanyuan Xu, Huixia Wang, Fei Jin, Zhengtao Shen, Deyi Hou, Green synthesis of layered double hydroxides (LDH) for the remediation of as and Cd in water and soil, Appl. Clay Sci. (2024) 107262.
[11] Hanhan Huang, Caifeng Xia, Derui Liang, Yuan Xie, Fanping Kong, Jinxiu Fu, Zhiwen Dou, Qinghua Yang, Wenjing Suo, Qian Zhang, Removal and magnetic recovery of heavy metals and pesticides from soil by layered double hydroxides modified biotite, Chem. Eng. J. (2022) 134113.
[12] Kok-Hui Goh, Teik-Thye Lim, Zhili Dong, Application of layered double hydroxides for removal of oxyanions: a review, Water Res. (2008) 1343–1368.
[13] Xin He, Pei Zhong, Xinhong Qiu, 2018. Remediation of hexavalent chromium in contaminated soil by Fe(II)-Al layered double hydroxide, Chemosphere (2018) 1157–1166.
[14] Hanhan Huang, Zhaosong Li, Haiyan Wang, Caifeng Xia, Pingke Yan, Qian Zhang, Zilin Meng, 2022. Adsorption performance of layered double hydroxides for heavy metals removal in soil with the presence of microplastics, J. Environ. Chem. Eng. (2022) 108733.
[15] Tingting Liu, Jiangrong Yang, Kaiyue Ji, Meiqi Zheng, Xiao Yang, Mingfei Shao, Haohong Duan, Xianggui Kong, 2024. Multiple anchor sites of CaFe-LDH enhanced the capture capacity to cadmium, arsenite, and lead simultaneously in contaminated water/soil: scalable synthesis, mechanism, and validation, ACS ES&T Eng (2024) 550–561.
[16] M.V. Bukhtiyarova, A review on effect of synthesis conditions on the formation of layered double hydroxides, J. Solid State Chem. (2019) 494–506.
[17] Karolina Rybka, Jakub Matusik, Artur Kuligiewicz, Tiina Leiviskä, Grzegorz Cempura, Temperature effect on the sorption of borate by a layered double hydroxide prepared using dolomite as a magnesium source, Appl. Surf. Sci. (2021) 147923.
[18] Ning Mao, Chun Hui Zhou, John Keeling, Saverio Fiore, Hao Zhang, Liang Chen, Gui Chen Jin, Ting Ting Zhu, Dong Shen Tong, Wei Hua Yu, Tracked changes of dolomite into Ca-Mg-Al layered double hydroxide, Appl. Clay Sci. (2018) 25–36.

[19] Karolina Rybka, Jakub Matusik, Artur Kuligiewicz, Tiina Leiviskä, Grzegorz Cempura, Surface chemistry and structure evaluation of Mg/Al and Mg/Fe LDH derived from magnesite and dolomite in comparison to LDH obtained from chemicals, Appl. Surf. Sci. (2021) 147923.
[20] Haoyang Ye, Shiyu Liu, Deyou Yu, Xuerong Zhou, Lei Qin, Cui Lai, Fanzhi Qin, Mingming Zhang, Wenjing Chen, Wenfang Chen, Regeneration mechanism, modification strategy, and environment application of layered double hydroxides: insights based on memory effect, Coord. Chem. Rev. (2022) 214253.
[21] Xue Duan, David G. Evans, Layered Double Hydroxides. Springer, 2006.
[22] Jialing Zhao, Luping Zhang, Shuwang Zhang, Wenying Yuan, Xing Fang, Qianqian Yu, Xinhong Qiu, Remediation of chromium-contaminated soil using calcined layered double hydroxides containing different divalent metals: temperatures and mechanism, Chem. Eng. J. (2021) 131405.
[23] E.A. Raymond, T.L. Tarbuck, G.L. Richmond, Isotopic dilution studies of the vapor/water interface as investigated by vibrational sum-frequency spectroscopy, J. Phys. Chem. B (2002) 2817–2820.
[24] Ping Huang, Aichun Dong, S. Winslow, Caughey. Effects of dimethyl sulfoxide, glycerol, and ethylene glycol on secondary structures of cytochrome c and lysozyme as observed by infrared spectroscopy. J, Pharmaceut. Sci. (1995) 387–392.
[25] Peter Kipkorir, Ling Tan, Jing Ren, Yufei Zhao, Yu-Fei Song, Intercalation effect in NiAl-layered double hydroxide nanosheets for CO 2 reduction under visible light, Chem. Res. Chin. Univ. (2020) 127–133.
[26] Peng Lyu, Lianfang Li, Xiaoya Huang, Jinni Xie, Jing Ye, Yunlong Tian, Jinli Huang, Changxiong Zhu, Ternary Ca-Mg-Al layered double-hydroxides for synergistic remediation of As, Cd, and Pb from both contaminated soil and groundwater: characteristics, effectiveness, and immobilization mechanisms. J, Hazard. Mater (2023) 130030.
[27] Shigeo Miyata, The syntheses of hydrotalcite-like compounds and their structures and physico-chemical properties I: the systems Mg^{2+}-Al^{3+}-NO_3^-, Mg^{2+}-Al^{3+}-C^{l-}, Mg^{2+}-Al^{3+}-ClO_4^-, Ni^{2+}-Al^{3+}-Cl^- and Zn^{2+}-Al^{3+}-Cl^-, Clay Clay Miner. (1975) 369–375.
[28] Shigeo Miyata, Teruhiko Kumura, Synthesis of new hydrotalcite-like compounds and their physico-chemical properties, Chem. Lett. (1973) 843–848.
[29] Donghua Zhang, Zhimeng Liu, Immobilization of chromium and cadmium in contaminated soil using layered double hydroxides prepared from dolomite, Appl. Clay Sci. (2022) 106654.
[30] Lisa Adhani, Ahmad Fauzi, Dovina Navanti, Tyastuti Sri Lestari, 2023. Rietveld refinement analysis of lampung natural zeolite catalyst impregnated Fe with diffraction method using MAUD software, Int. J. Adv. Sci. Eng. Inf. Technol. (2023) 2088–5334.
[31] F. Delorme, A. Seron, M. Bizi, V. Jean-Prost, D. Martineau, Effect of time on the reconstruction of the $Mg_4Al_2(OH)_{12}CO_3{\cdot}3H_2O$ layered double hydroxide in a Na_2CO_3 solution. J, Mater. Sci. (2006) 4876–4882.
[32] Xiaoqian Jiang, Binggang Yan, Jiayu Chen, Wenyan Li, Jiawei Hu, Yuntao Guan, Transport and retention of phosphorus in soil with addition of Mg-Al layered double hydroxides: effects of material dosage, flow velocity and pH, Chem. Eng. J. (2019) 122154.
[33] Wenying Yuan, Qianqian Yu, Jinyi Chen, Xinhong Qiu, Immobilization of Cr (VI) in polluted soil using activated carbon fiber supported FeAl-LDH. Colloid, Surfaces A (2022) 129884.
[34] J. Cáliz, G. Montserrat, E. Martí, et al., Emerging resistant microbiota from an acidic soil exposed to toxicity of Cr, Cd and Pb is mainly influenced by the bioavailability of these metals[J], Soils Sediments 13 (2013) 413–428.
[35] Y. Chen, Y. Jiang, H. Huang, et al., Long-term and high-concentration heavy-metal contamination strongly influences the microbiome and functional genes in Yellow River sediments[J], Sci. Total Environ. (2018) 637–638, 1400-1412.
[36] C.S. Sheik, T.W. Mitchell, F.Z. Rizvi, et al., Exposure of soil microbial communities to chromium and arsenic alters their diversity and structure[J], PLoS One (2012).
[37] N.H. Youssef, M.S. Elshahed, Diversity rankings among bacterial lineages in soil[J], ISME J. 3 (3) (2009) 305–313.
[38] C.S. Sheik, W.H. Beasley, M.S. Elshahed, et al., Effect of warming and drought on grassland microbial communities[J], ISME J. 5 (10) (2011) 1692–1700.
[39] X.F. Luo, M.Y. Liu, Z.X. Tian, et al., Physiological tolerance of black locust (Robinia pseudoacacia L.) and changes of rhizospheric bacterial communities in response to Cd and Pb in the contaminated soil[J], Environ. Sci. Pollut. Res. Int. 31 (2) (2024) 2987–3003.
[40] Shigeo Miyata, 1983. Anion-exchange properties of hydrotalcite-like compounds, Clay Clay Miner. (1983) 305–311.
[41] Khalil Ahmad, Ijaz A. Bhatti, Majid Muneer, Munawar Iqbal, Zafar Iqbal, 2012. Removal of heavy metals (Zn, Cr, Pb, Cd, Cu and Fe) in aqueous media by calcium carbonate as an adsorbent, International Journal of Chemical and Biochemical Sciences (2012) 48–53.
[42] Bin Hua, Baolin Deng, Edward C. Thornton, John Yang, James E. Amonette, 2007. Incorporation of chromate into calcium carbonate structure during coprecipitation, Water Air Soil Pollut. (2007) 381–390.
[43] M. Salvi Anna, E. Castle James, F. Watts John, Elio Desimoni, Peak fitting of the chromium 2p XPS spectrum, Appl. Surf. Sci. (1995) 333–341.
[44] Zhenhui Li, Xing Fang, Wenying Yuan, Xiaoxuan Zhang, Junxia Yu, Jinyi Chen, Xinhong Qiu, Preparing of layered double hydroxide- alginate microspheres for Cr(VI)-contaminated soil remediation, Colloid. Surface. (2023) 130655.